UDC 53.086 621.9.048.4

DOI: 10.17580/cisisr.2018.02.12

PROTECTIVE COATINGS PRODUCED BY ELECTRO-SPARK DEPOSITION WITH TiCNiCr-(Eu_2O_3) ELECTRODES

Ph. V. Kiryukhantsev-Korneev[1], A. D. Sytchenko[1], A. E. Kudryashov[1], E. A. Levashov[1]

[1] *National University of Science and Technology "MISiS" (Moscow, Russia)*

E-mail: kiruhancev-korneev@yandex.ru

AUTHOR'S INFO

Ph. V. Kiryukhantsev-Korneev, Cand. Eng., Associate Prof., Department of Powder Metallurgy and Functional Coatings; Leading Researcher, Scientific and Educational Center SHS MISiS-ISMAN,
A. D. Sytchenko, Laboratory Assistant, Scientific and Educational Center SHS MISiS-ISMAN,
A. E. Kudryashov, Cand. Eng., Leading Researcher, Scientific and Training Center SHS MISiS-ISMAN,
E. A. Levashov, Dr. Eng., Prof., Head of the Department of Powder Metallurgy and Functional Coatings; Director, Scientific and Educational Center SHS MISiS-ISMAN.

Key words:

TiC–Ni, europium oxide, electro-spark alloying, steel, coating, structure, hardness, friction coefficient, mechanical and tribological properties, corrosion resistance, oxidation resistance, oxidation kinetics.

ABSTRACT

This paper examines coatings deposited on 40x (analog of 5140) steel substrates by electro-spark alloying with TiCNiCr and TiCNiCr–Eu_2O_3 electrodes. The techniques of X-ray phase analysis, scanning electron microscopy, energy dispersive X-ray spectroscopy and glow-discharge optical emission spectroscopy were applied to analyze the structure, as well as the elemental and phase compositions of the coatings. The mechanical and tribological properties of the coatings were analyzed with the help of nanoindentation and pin-on-disk tests. The coatings were also subjected to electrochemical testing and annealing. The obtained results did not reveal any significant difference between the coatings with Eu_2O_3 in terms of the structure and friction coefficient. However, in terms of heat and corrosion resistance, the coatings with Eu_2O_3 outperform the basic ones. The doped coatings had a more than 20 times lower corrosion current and almost 2 times lower the oxidation number compared with undoped coatings. It is shown that due to the developed coatings the steel parts can be 2.5 times harder, 7 times more wear resistant (with half as high the friction coefficient), more than 20 times more corrosion resistant, and 18 times more heat resistant.

1. Introduction

Operational wear of machine parts and steel structures poses a serious problem which can entail considerable energy and financial losses. Wear can be reduced by simply modifying the surface of machine parts through deposition of protective coatings [1]. Electro-spark alloying (ESA) provides one of the popular deposition techniques offering such advantages as high adhesion, a possibility to do local surface processing (also on large parts), low thermal impact on the substrate, relative simplicity of the process, the lack of strict surface preparation specifications, high reliability of equipment [2].

The most common protective coatings include WC–Co cemented carbides [3–5]. The use of tungsten-free cemented carbides (e.g. titanium carbide based [6–9]) would help significantly reduce the cost of reduction and hardening. When using TiC–Ni electrodes, titanium carbides and a solid solution of nickel in iron form in the coating resulting in a sound deposit free of micro- or macrocracks [7]. If TiC–Ni electrodes are replaced with TiC–NiCr electrodes, the resultant ESA coatings would have enhanced mechanical and tribological properties [8] and heat resistance [9]. Additions of NbC, WC, ZrO_2 and Al_2O_3 to electrodes help modify the structure of resultant coatings by making the TiC phase grains finer, which leads to an almost 30% increase in microhardness, a 25% increase in heat resistance, and a reduction of the friction coefficient from 0.26 to 0.15 [9].

Use of rare earth metals (REM) and their compounds as alloying elements for ESA electrodes has not been properly studied and is of great interest. It is a well-known fact that the use of REMs helps decrease the electronic work function and increase the emission current [10, 11]. And Eu has the lowest work function equal to 2.5 eV [12]. A study [13] showed that the addition of REMs to the Stellit 6 coating produced by plasma cladding can increase the hardness of the coating by more than 30%, which is due to the effect produced on the parameters of gas discharge and the coating structure. Apart from the above effects, the addition of REMs can enhance the properties of coatings: mechanical strength [14], hardness [15], fracture toughness [16], corrosion resistance [17], residual stresses, and modulus of elasticity [18]. In our previous study [19], we found that the addition of 1 at.% Eu_2O_3 to the TiCNiCr electrode extends the pulse duration by 19% and increases the coating rate. This research aims to thoroughly examine the structure and properties of coatings produced on 40x steel substrates by electro-spark alloying with TiCNiCr and TiCNiCr-Eu_2O_3 electrodes.

2. Materials and Methods

Powders of titanium carbide, nickel, chromium and europium oxide were used as primary components for electrodes. The powders were mixed in an Aktivator-2S planetary centrifugal mill in an argon atmosphere for 5 minutes. A hydraulic press was used for pressing the powder at 7.5 MPa. The resultant briquettes were roasted in Al_2O_3 bed

in a VE-3-16 vacuum furnace by NPP VakETO, Russia at 1,450 °C for 60 minutes. The 4×4×50 mm TiCNiCr and TiCNiCr-Eu_2O_3 electrodes were analyzed by scanning electron microscopy (SEM) and energy dispersive spectroscopy (EDS) on a Hitachi S-3400N microscope with a Noran 7 Thermo EDS; by X-ray phase analysis (XRD) on a D8 ADVANCE diffractometer by Bruker, Germany, using Cu-K_α radiation. The results are given in Table 1. It was established that the electrodes contain TiC phase grains, a solid solution of NiCr and Eu_2O_3 (if it is a doped electrode). Ø30×5 mm 40x polished steel discs were used as substrates. Before deposition, the substrates were subjected to ultrasonic cleaning in isopropyl alcohol for 5 minutes. A UZDN-2T unit was used for it.

Electro-spark alloying was performed in an Alier-Metal 303 unit, which is controlled by a microprocessor and designed as an independent generator (i.e. the current pulses are not synchronized with the touch-down frequency). Deposition was carried out in an Ar atmosphere at 10^5 Pa in the following conditions: current — 120 A, voltage — 20 V, pulse duration — 20 μs, frequency — 640 Hz, duty factor — 1.3%, deposition time — 3 min/cm^2. Two deposition modes were applied: normal polarity (NP) mode, when the electrode functions as an anode; and reverse polarity (RP) mode, when the electrode functions as a cathode.

The above mentioned methods of SEM, EDS and XRD were used to analyse the morphology, as well as the elemental and phase composition of the coatings. The mechanical properties of the coatings, such as hardness (H), modulus of elasticity (E) and elastic recovery (W), were analyzed with the help of a Nano Hardness Tester by CSM Instruments equipped with a Berkovich tip at 4 mN. Tribological tests were performed on a Tribometer by CSM Instruments in a rod/disc mode. The specimens were tested in contact with a 6 mm Al_2O_3 ball at room temperature, the linear speed of 10 cm/s, and the normal load of 5 N. The wear tracks and surface roughness of the ESA coatings were analyzed with the help of a WYKO NT 110 optical profilometer. The electrochemical properties of the coatings were analyzed with the help of a VoltaLab 50 three-electrode cell with a potentiostat by Radiometer Analytical. The tests were carried out in a 1N H_2SO_4 solution with an Ag/AgCl comparison electrode and a Pt auxiliary electrode. All potentials were recalculated against standard hydrogen electrode. The Tafel equation was applied for corrosion current density (i_{cor}) calculations. As part of heat resistance test, the coatings were loaded in a SNOL 7.2/1200 (Umega) pre-heated furnace and air annealed at 400, 500, 600, 700 and 800 °C with an isothermal time of 1 h for each temperature. After annealing, specimens of the normal polarity coatings were analyzed with a Profiler-2 glow-discharge optical emission spectrometer (GDOES) by HORIBA Jobin Yvon, France. The reverse polarity specimens were not analyzed because of excessive roughness. The coating oxidation kinetics was also analyzed by gravimetric method using KERN 770 analytical balances after 10, 30, 60 and 180 minutes of annealing at each temperature. The following formula was used to calculate the oxidation number (Δm_S), which indicates how much the weight of the specimen changes due to oxidation per unit of area: $\Delta m_S = (m_1 - m_0)/S_0$, where m_0 — initial weight of the specimen, g; m_1 — the weight of the specimen with oxidation products, g; S_0 — surface area of the specimen, m^2.

Table 1. **Elemental Composition of Powder Mixtures, Electrodes and Coatings**

Composition, wt%							
#	Name	Ti	C	Ni	Cr	Eu	Fe
Powder mixture, wt%							
1	TiCNiCr	68.7	17.2	5.4	8.7	–	–
2	TiCNiCr–Eu_2O_3	65.8	15.2	5.1	8.2	5.7	–
Electrode (EDS), wt%							
1	TiCNiCr	71.0	19.0	2.9	7.1	–	–
2	TiCNiCr–Eu_2O_3	69.5	15.6	2.5	6.9	5.7	–
Coating, wt%							
1	TiCNiCr NP	31.7	11.3	3.6	6.8	–	46.6
2	TiCNiCr–Eu_2O_3 NP	34.4	11.0	4.3	6.9	6.5	36.9
3	TiCNiCr RP	36.7	14.2	3.6	5.5	–	40
4	TiCNiCr–Eu_2O_3 RP	33.9	11.9	3.1	4.9	11.9	34.3

3. Results and Discussion

3.1. Elemental Composition

The specimen numbers and the elemental compositions of the ESA coatings produced with the TiCNiCr and TiCNiCr-Eu_2O_3 electrodes in normal and reverse polarity modes are given in **Table 1**. For coatings 1 and 2, the concentrations of Ti, C, Ni, and Cr differed by 2.7, 0.3, 0.7 and 0.1 wt%, correspondingly. Addition of Eu_2O_3 expectedly resulted in reduced concentrations of elements in the electrode, but the ratio between them stayed the same. When going from coating 1 to coating 2, the concentration of Fe as the key component of the substrate would drop by 21%, which can be attributed to a greater thickness of coating 2 due to the addition of Eu_2O_3. In the case of coatings 3 and 4, the difference in the concentration of the substrate component was 14%.

A GDOES study showed an expressed concentration gradient present in the coatings. The signal produced by Fe is monotonely increasing from the surface of the coating to the substrate, while the concentrations of the electrode components are decreasing (**Fig. 1**). Such results are typical of ESA coatings. The GDOES also confirmed the presence of Eu in the coatings that were produced with the TiCNiCr–Eu_2O_3 electrode.

3.2. Microstructure and Phase Composition

Fig. 1 shows X-ray patterns of the coatings. Peaks were identified for all the coatings, which are related to the reflections from planes (111), (200), (220), (311), (222) of

the titanium carbide FCC phase. It was established that the peaks corresponding to planes (110) and (211) belong to the α-Fe phase. Peaks of the solid solution of Ni and Cr in iron are also present. In the case of ESA coatings 2 and 4 produced with a doped electrode, peaks in the positions $2\theta = 31.4$ and 32.4 can be found in the X-ray patterns, which are typical of Eu_2O_3 [20, 21].

The Scherrer equation was used to calculate the size of titanium carbide crystallites. The results showed that the crystallite size determined on the basis of line (111) broadening, is the same for coatings 1–4 and is equal to 22 nm. Calculations performed for the strongest line (200) showed that, when going from coating 1 to coating 2, the TiC crystallite size stayed the same and was equal to 30 nm, whereas for line (220) the crystallite size reduced from 25 to 20 nm. The same refers to coatings 3 and 4, for which the TiC crystallite size on line (200) reduced from 30 to 18 nm following the addition of Eu_2O_3. Calculations performed on the other lines, which have a lower intensity, showed either similar results or a slightly bigger size of the crystallites induced by doping. It should be noted that base phase grain refinement is characteristic of europium oxide [22]. The Eu_2O_3 phase grain size for coatings 2 and 4 was approximately 20 nm.

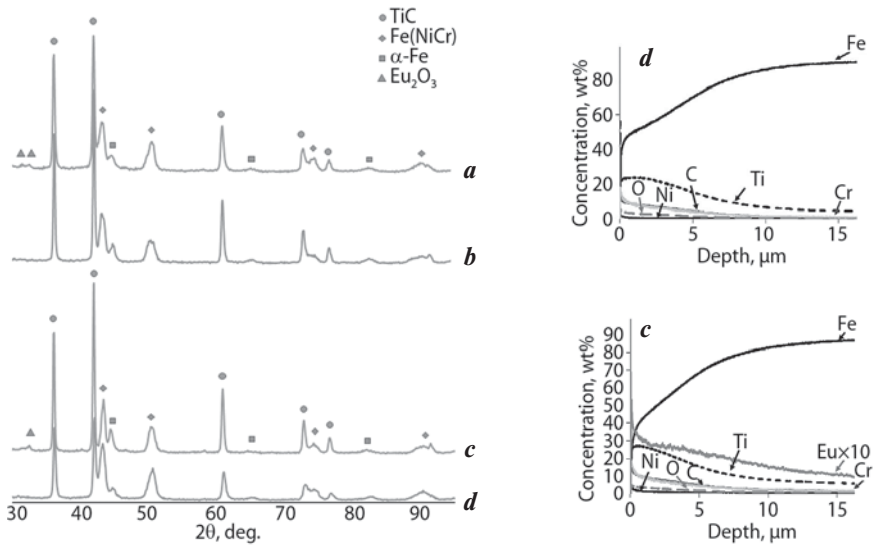

Fig. 1. X-ray patterns (left) and elemental profiles (right) of the coatings: *a* — coating 4; *b* — coating 3; *c* — coating 2; *d* — coating 1

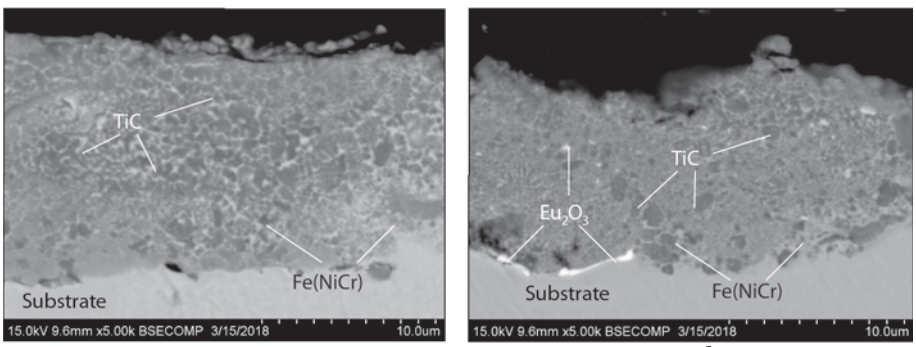

a *b*

Fig. 2. SEM data for coating cross-sections: *a* — coating 1; *b* — coating 2

The lattice parameter of the undoped coatings was 0.429–0.430 nm, and the coatings with Eu_2O_3 had slightly different values, which were within 0.430–0.431 nm. These are slightly lower than for the volume TiC (0.433 nm). The smaller lattice parameter can be attributed to the presence of tensile stresses [23] or a deviation from the stoichiometric composition of the TiC phase [24].

The sectional views of the coatings (**Fig. 2**) show titanium carbide grains and areas of the solid solution of Fe(NiCr), and in the case of coatings 2 and 4 — also Eu_2O_3 grains (lighter areas in the SEM images). Europium oxide can be found both at the coating/substrate boundary and in the coating. With the help of micrographs, the TiC grain size was estimated to be between 10 and 70 nm. No significant structural difference was found between coatings produced under different polarities. According to EDS data, the composition of TiC and Eu_2O_3 phases was close to stoichiometric. The concentrations of Ni and Cr in the solid solution were around 20 and 25%, correspondingly.

The authors established that the roughness of coatings is mainly affected by polarity. For coatings 1 and 2, roughness R_a was 2.95 and 2.22 μm, and for coatings 3 and 4 — $R_a = 5.10$ μm and $R_a = 5.98$ μm, appropriately. Transition from NP to RP equates to a 1.7–2.7 time increase in roughness. The addition of Eu_2O_3 produces a smaller effect on roughness.

3.3. Mechanical Properties

The coatings cross-sections were used for nanoindentation tests. The results are given in **Table 2**. Coating 1 had the following characteristics: hardness — 23.7 GPa, modulus of elasticity — 252 GPa, elastic recovery — 66%. Characteristics of coating 2: $H = 20.8$ GPa, $E = 230$ GPa, $W = 62\%$. When going from coating 3 to coating 4, the above characteristics would drop by 29, 14 and 11%. Thus, the mechanical properties of the basic coatings 1 and 3 superseded those of coatings 2 and 4 doped with Eu_2O_3. It should be noted that in terms

Table 2. **Mechanical, tribological and electrochemical characteristics of coatings and substrate**

No.	Coating	*H*, GPa	*E*, GPa	*W*,%	φ, mV	i_{cor}, mA/cm²	*f*	*Vw*·10⁻⁵, mm³/N/m
1	TiCNiCr NP	23.7	252	66	179	0.84	0.33	< 0.4
2	TiCNiCr–Eu_2O_3 NP	20.8	230	62	178	0.49	0.36	< 0.4
3	TiCNiCr RP	26.5	333	62	174	4.21	0.30	< 0.4
4	TiCNiCr–Eu_2O_3 RP	18.9	285	55	182	0.19	0.34	< 0.4
5	40X steel	11.0	224	35	190	4.50	0.78	2.8±0.2

H — hardness, GPa; *E* — modulus of elasticity, GPa; *W* — elastic recovery,%; φ — corrosion potential, mV; i_{cor} — corrosion current density, mA/cm²; *f* — friction coefficient; *Vw* — wear rate, mm³/N/m.

of hardness, all the coatings outperformed the 40x substrate and had high elasticity and ductility. The decrease of the modulus of elasticity E was due to the presence of the substrate component in the coating. We should note here that a low modulus of elasticity combined with a high hardness can contribute to wear resistance in coatings [25]. According to literature, the hardness of ESA coatings produced with TiC–Ni electrodes is 13.9 GPa [7]. The addition of Cr makes the hardness rise to 15 GPa [8]. After doping of the basic TiC–Ni composition with different elements, such as Mo, Al_2O_3 and ZrO_2, the hardness of coatings can rise to 17 GPa [7]. Correspondingly, the ESA coatings produced in this research have superior mechanical properties compared with the coatings from the previous studies.

3.4. Tribological Properties

Fig. 3 shows that the friction coefficient depends on the distance. Coatings 1 and 2 had a close initial friction coefficient of 0.2. The friction coefficient of coatings 1 and 2 would be increasing up during the entire test reaching around 0.4. The average values of the friction coefficient for coatings 1 and 2 were 0.33 and 0.36, correspondingly. Coating 3 demonstrated the lowest and the most consistent friction coefficient with an average value of 0.30. The friction coefficient of coating 4 in the distance of up to 100 mm was 0.30, after that distance the average value of the friction coefficient increased to 0.34. After the tribological tests, the specimens were tested with an optical surface tester, which produced 2D and 3D profiles of the tribocontact areas. Figure 3 also shows 2D profiles of the substrate and of coating 1. The substrate profiles clearly show that the depth of the track is 3 μm. In the case of the ESA coating, the wear is almost indistinguishable and the wearing depth is comparable with the surface roughness (R_a = = 2.95 μm). If the wearing zone is almost indistinguishable in the coating 1 profiles, it is not even possible to identify signs of wear on the other coatings. However, by looking at the wear track on coating 1, which is more pronounced than on the other specimens, one can conclude that the wear rate of coatings 1–4 does not exceed $0.4 \cdot 10^{-5}$ mm³/(Nm). Consequently, the addition of europium oxide only has a slight effect on the tribological properties of the coatings. The friction coefficient and the wear rate, to a greater extent, depend on the surface roughness of coatings. A substrate without coating tested under the same conditions had a friction coefficient of 0.78 and a wear rate of $3 \cdot 10^{-5}$ mm³N⁻¹m⁻¹ (the data are shown in Fig. 3).

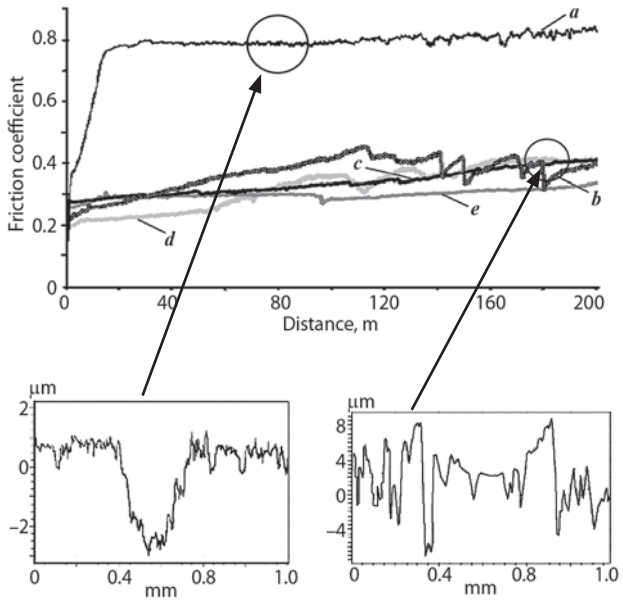

Fig. 3. Friction coefficient of coatings and substrate:
a — substrate; *b* — coating 2; *c* — coating 4; *d* — coating 1; *e* — coating 3
The inserted graphs show the wear track profiles of the substrate and of coating 1

3.5. Electrochemical Properties

The results of electrochemical analysis (corrosion potential φ, corrosion current density i_{cor}) are given in Table 2. The corrosion potentials of all coatings deposited on steel substrate is consistent with the free corrosion potential of iron. It is because the electrolyte, through cracks and defects in the coating, reaches the substrate causing an abundant dissolution of iron.

Polarization curves helped determine corrosion current density of all the coatings and the substrate (Table 2). For coating 1, i_{cor} was 0.84 mA/cm², which is 42% higher than the corrosion current density of coating 2 (0.49 mA/cm²). The corrosion current density of coating 3 was consistent with that of iron. Coating 4 had the lowest corrosion

current density — 0.19 mA/cm². This can be due to both a greater thickness of the coating and the positive effect of the REM addition [26, 27], the concentration of which is the highest in this coating. Coatings with an optimum composition would lead to reduced i_{cor}, which was 20 times lower compared with the substrate.

Table 3. **Coating oxidation number and rate**

#	Coating	500 °C		600 °C		700 °C	
		Δm_S, g/m²	$V_{oxid} \cdot 10^3$, g/min	Δm_S, g/m²	$V_{oxid} \cdot 10^3$, g/min	Δm_S, g/m²	$V_{oxid} \cdot 10^3$, g/min
1	TiCNiCr NP	1.162	0.045	1.211	0.046	2.289	0.088
2	TiCNiCr–Eu_2O_3 NP	1.031	0.039	1.062	0.040	2.938	0.111
3	TiCNiCr RP	1.484	0.053	1.531	0.054	3.741	0.133
4	TiCNiCr–Eu_2O_3 RP	1.337	0.048	1.373	0.050	1.926	0.070

Δm_S — oxidation number, g/m²; V_{oxid} — oxidation rate, g/min.

3.6. Heat Resistance

A common method to analyze heat resistance involves investigation of the kinetics of oxidation. During oxidation, C, B and N can burn out forming volatile compounds with oxygen. That is why, for the purposes of this research, two methods were used to analyze heat resistance: by changing weight and by changing concentrations of oxygen and carbon in the coatings, which were determined based on the elemental profiles of annealed coatings.

Experiments conducted at 400 °C failed to identify the oxidation mechanism due to low values (less than 0.2 g/m²) and a great variability of Δm_S in the case of coatings 2 and 4 with the Eu_2O_3 addition. After protective oxides [28] formed on the surface in the first 10–30 min, coatings 1 and 3 without the addition experienced almost no oxidation. Analysis of the kinetic dependencies of oxidation in specimens at 500, 600 and 700 °C (data for 600 °C are given in **Fig. 4** as an example) helped understand that all the coatings (1–4) have a linear oxidation kinetics. **Table 3** contains aggregate data on the oxidation rates and numbers as determined based on the kinetic curves. The curves clearly show that because of the Eu_2O_3 addition these values drop by 7–13% at 500 °C and 600 °C, and the normal polarity coatings benefit more. At 700 °C, coating 4 with the Eu_2O_3 addition had the lowest oxidation rate (i.e. 1.926 g/m²). The substrate tested at 600 °C gave values that exceeded those for coatings 1–4 by 18 times (see Fig. 4).

A GDOES study of the primary coatings and the coatings after annealing indicated that in their initial state coatings 1 and 2 have almost the same concentrations of carbon. Elemental profiles show a weaker carbon signal at 400–600 °C compared with the initial level, which is the result of carbon burn-out. No difference was observed between coatings 1 and 2 in terms of the degree to which the carbon signal dropped. At the same time, following annealing at 700 °C, a 25% difference was observed in carbon concentration between the two coatings. This trend continued with further annealing at 800 °C, and coating 2 had a lower carbon burn-out rate.

Based on the GDOES data, bar graphs were built which indicate the oxygen penetration depth in coatings 1 and 2 at 500, 600, and 700 °C. The oxidation depth in coatings 1 and 2 after annealing at 500 °C was almost the same and was within 5–6 μm. At the same time, following the addition of Eu_2O_3 at 600°C and 700°C, the oxygen penetration depth would be 20% smaller. As indicated by both tests, the coatings with Eu_2O_3 proved

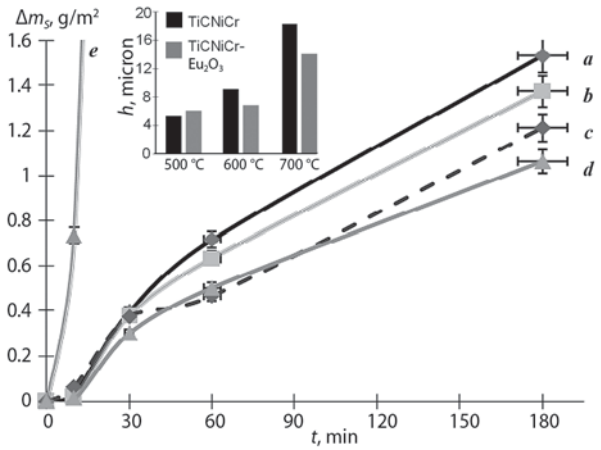

Fig. 4. Relationship between the specimens oxidation number and time (T = 600 °C):
a — coating 3; *b* — coating 4; *c* — coating 1; *d* — coating 2; *e* — substrate.
The inserted graph shows how the oxygen penetration depth (*h*) in coatings 3 and 4 depends on the temperature, as indicated by GDOES

to have a better heat resistance than undoped coatings, with the positive effect being more pronounced at higher temperatures.

Conclusion

Coatings were produced on 40x steel by electro-spark alloying with TiCNiCr and TiCNiCr–Eu_2O_3 electrodes in normal and reverse polarity modes. The resultant coatings contained phases of titanium carbide, a solid solution of nickel and chromium in iron, as well as Eu_2O_3 (due to the TiCNiCr–Eu_2O_3 electrode). Addition of europium oxide would lead to a hardness decrease from 23–27 GPa to 18–20 GPa while not producing any noticeable effect on the friction coefficient. At the same time, it would lead to enhanced corrosion and heat resistances. Compared with undoped coatings, the coatings produced with the TiCNiCr–Eu_2O_3 electrode in reverse polarity mode and having the maximum amount of Eu (around 12%) had a lower corrosion current density in H_2SO_4 (0.19 versus 4.2 mA/cm²) and a lower oxidation number at 700 °C (1.9 versus 3.7 g/min). Steel parts with ESA coatings can be 2.5 times harder, 7 times more wear resistant (with half as high the friction coefficient), more than 20 times more corrosion resistant, and 18 times more heat resistant.

This research was funded by the Ministry of Education and Science of Russia (Assignment No. 11.7172.2017/8.9).

The authors thank A. N. Sheveyko and N. V. Shvyndina for their support with electrochemical testing and structural analysis of the coatings.

REFERENCES

1. Gerasimova A. A., Radyuk A. G. The improvement of the surface quality of workpieces by coating. *CIS Iron and Steel Review*. 2014. Vol. 9. pp. 33–35.
2. Verkhoturov A. D., Mukha I. M. Electrospark alloying technology. Kiev : Tekhnika. 2002. 182 p.
3. Agudelo-Morimitsu L. C., De La Roche J., Rudena A., Escobar D., Restrepo-Parra E. Effect of substrate temperature on the mechanical and tribological properties of W/WC produced by DC magnetron sputtering. *Ceramics International*. 2014. Vol. 40. pp. 7037–7042.
4. Nikolenko S. V., Kuzmenko A. P., Timakov D. I., Abakymov P. V. Nanostructuring a steel surface by electrospark treatment with new electrode materials based on tungsten carbide. *Surface Engineering and Applied Electrochemistry*. 2011. Vol. 47. pp. 217–224.
5. Villiers H. L. Lovelock, powder/processing/structure relationships in WC–Co thermal spray coatings: a review of the published literature. *Journal of Thermal Spray Technology*. 1998. Vol. 7. pp. 357–373.
6. Nikolenko S. V., Syuy N. A., Burkov A. A. Investigation of microstructure and properties of coatings on the steel 45, applied by TiC — Ni — Mo based electric discharge deposition. *Tsvetnye Metally*. 2017. No. 4. pp. 69–75.
7. Panteleenko F. I., Sarantsev V. V., Stolin A. M., Bazhin P. M., Azarenko E. L. Formation of composite coatings based on titanium carbide via electrospark alloying. *Surface Engineering and Applied Electrochemistry*. 2011. Vol. 47. pp. 336–348.
8. Andreev A. V., Litovchenko I. Y., Korotaev A. D., Borisov D. P. Thermal Stability of Ti–C–Ni–Cr and Ti–C–Ni-Cr–Al–Si Nanocomposite Coatings. *Journal of Physics: Conference Series*. 2015. Vol. 652. pp. 012057.
9. Levashov E. A., Kudryashov A. E., Vakaev P. V., Malochkin O. V., Gammel F., Suchentrunk R., Moore J. J. The prospect of Nanodispersive Powders Application in Surface Technologies. *Surface and Coating Technologies*. 2004. Vol. 180-181. pp. 347–351.
10. Izraelyants K. R., Orlov A. P., Ormont A. B., Chirkova E. G. Effect of the cesium and potassium doping of multiwalled carbon nanotubes grown in an electrical arc on their emission characteristics. *Physics of the Solid State*. 2017. Vol. 59. pp. 838–844.
11. Kong J. T., Shi S. Y., Kong L. C., Zhu X. P., Ni J. R. Preparation and characterization of PbO_2 electrodes doped with different rare earth oxides. *Electrochimica Acta*. 2007. Vol. 53. pp. 2048–2054.
12. Hua G., Li D. Generic relation between the electron work function and Young's modulus of metals. *Applied Physics Letters*. 2011. Vol. 99. pp. 041907.
13. Fang Y., Cui X., Cai Z., Wang C., Jin G. Influence of La_2O_3 addition on nano indentation hardness and residual stress of Stellite 6 coating prepared by plasma cladding. *Journal of Rare Earths*. 2018. DOI: 10.1016/j.jre.2018.03.008.
14. Zhao T., Xun C., Wang S. X., Zheng S. A. Effect of CeO_2 on microstructure and corrosive wear behavior of laser-cladded Ni/WC coating. *Thin Solid Film*. 2000. Vol. 379. pp. 128–132.
15. Li J., Luo X., Li G. J. Effect of Y_2O_3 on the sliding wear resistance of TiB/TiC-reinforced composite coatings fabricated by laser cladding. *Wear*. 2014. Vol. 310. pp. 72–82.
16. Li J., Wang H. P., Li M. P., Yu Z. S. Effect of yttrium on microstructure and mechanical properties of laser clad coatings reinforced by in situ synthesized TiB and TiC. *Journal of Rare Earths*. 2011. Vol. 29. pp. 477–483.
17. Zhu R., Li Z., Li X., Sun Q. Microstructure and properties of the low-power-laser clad coatings on magnesium alloy with different amount of rare earth addition. *Applied Surface Science*. 2015. pp. 353–405.
18. Kiryukhantsev-Korneev Ph. V., Sheveyko A. N., Shvindina N. V., Levashov E. A., Shtansky D. V. Comparative study of Ti–C–Ni–Al, Ti–C–Ni–Fe, and Ti–C–Ni–Al/Ti–C–Ni–Fe coatings produced by magnetron sputtering, electro-spark deposition, and a combined two-step process. *Ceramics International*. 2018. Vol. 44. pp. 7637–7646.
19. Kiryukhantsev-Korneev Ph. V., Sytchenko A. D., Kudryashov A. E., Levashov E. A., Shtansky D. V. The Effect of Eu_2O_3 Additive to the TiCNiCr Electrode on the Formation of Electrospark Coatings. *Technical Physics Letters*. 2018. Vol. 44. pp. 753–755.
20. Ahlawat R., Rani N., Goswami B. Synthesis and characterizations of Eu_2O_3 nanocrystallites and its effect on optical investigations of Eu^{3+}, Eu^{2+}: SiO_2 nanopowder. *Journal of Alloys and Compounds*. 2018. Vol. 743. pp. 126–135.
21. Niu T., Zhang P., Zheng G., Liu l., Deng J., Jin Y., Jiao Z., Sun X. Tuning the charge transition process of Eu_2O_3 nanorods by coupling with Ag nanoparticles for enhanced photocatalytic performance. *Journal of Environmental Chemical Engineering*. 2017. Vol. 5. pp. 2930–2936.
22. Hui Y., Zhao S. M., Xu J. Y. Doping concentration of Eu^{3+} as a fluorescence probe for phase transformation of zirconia. *Journal of Rare Earths*. 2015. Vol. 33. pp. 717–725.
23. Paustovskii A. V., Gubin Yu. V. Stresses in coatings obtained by electro-spark alloying and laser processing (review). *Materials Science*. 1997. Vol. 33. pp. 770–776.
24. Chen Z., Zhou Y. Surface modification of resistance welding electrode by electrospark deposited composite coatings: part I. Coating characterization. *Surface Coating Technology*. 2006. Vol. 201. pp. 1503–1510.
25. Leyland A., Matthews A. On the significance of the H/E ratio in wear control: a nanocomposite coating approach to optimised tribological behavior. *Wear*. 2000. Vol. 246. pp. 1–11.
26. Murthy T. K. S., Gupta C. K. Rare earth resources, their extraction and applications. *The Science and Technology of Rare Earth Materials*. 1980. pp. 3–23.
27. Ozgurluk Y., Doleker K. M., Ahlatci H., Karaoglanli A. C. Investigation of hot corrosion behavior of thermal barrier coating (TBC) systems with rare earth contents. *Arabian Journal of Geosciences*. 2018. 11:267.
28. Lavrenko V. A., Glebov L. A., Pomitkin A. P., Chuprina V. G., Protsenko T. G. High-temperature oxidation of titanium carbide in oxygen. *Oxidation of Metals*. 1975. Vol. 9. pp. 171–179.